Anti-jamming Techniques for Multichannel SAR Imaging

Luke Rosenberg[a,b,c] and Doug Gray[a,b]

(a) University of Adelaide, Australia (b) Cooperative Research Center for Sensor, Signal and Information Processing (CSSIP) (c) Defence, Science and Technology Organisation (DSTO)

email: luker@eleceng.adelaide.edu.au, dgray@eleceng.adelaide.edu.au

Abstract

An airborne broadband jammer present in the mainbeam of a Synthetic Aperture Radar (SAR) can potentially destroy a large region of the SAR image. In addition to this, multipath reflections from the ground, known as hot-clutter or terrain scattered interference will add a non-stationary interference component to the image. The goal of interference suppression for SAR is to successfully suppress these interferences while not significantly effecting the image quality by blurring, reducing the resolution or raising the sidelobe level. This paper provides an analysis of the degradation from hot-clutter, the limited restoration that slow-time Space Time Adaptive Processing (STAP) can provide and how fast-time STAP can improve the final image.

1 Introduction

Coherent SAR imaging can be very sensitive to additive noise and an airborne broadband jammer has the potential to cause it to be effectively useless. The interference from an airborne jammer can be modelled by a direct-path signal and multipath reflections from the ground. The direct-path of the jammer signal is defined by a narrow azimuth region and requires spatial degrees of freedom for effective cancellation. It has been shown that by combining the multichannel data from multiple pulses (slow-time) and performing slow-time STAP, much greater suppression is possible [1]. On the other hand, due to the diffuse reflection from the ground, the hot-clutter component is spread in azimuth and its properties can change rapidly with time, even over several pulses. While this technique works well for suppressing signals which are narrow in azimuth, as the hot-clutter becomes more dominant, interference contributions spread over azimuth and the recovered image is blurry and poor quality.

Thus, to remove the effect of non-stationarity between pulses, cancellation must occur before azimuth processing and therefore requires adaption using fast-time samples from within each pulse. An effective method for removing stationary and non-stationary interferences for a general airborne radar is to combine the spatial and fast-time samples into a space/fast-time adaptive processor [2]. A third comparison is performed with results from optimal fast-time STAP. While the results show improvement over slow-time STAP, there are now two new side-effects similar to those described in [3]. The first is a 'training modulation' due to different training sets used in estimation of the jammer covariance matrix and the second is a 'coherence modulation' which results from the incoherency of the hot-clutter. The consequence of these side-effects are to increase the sidelobe level of the target signal and cause it to blur across doppler bins.

2 Signal and Hot-clutter Model

Consider a SAR travelling along the y-axis, imaging a patch in the slant-plane $x \in [X_c - X_0, X_c + X_0]$, $y \in [-Y_0, Y_0]$. After range processing, the received signal at the n^{th} antenna from the k^{th} patch (x_k, y_k) with Radar Cross Section (RCS) σ_k is given by,

$$s_{n,k}(t,u) = \sigma_k \exp\big[-j\omega_c \tau_{n,k}(u)\big] \operatorname{sinc}\big[B\pi(t - \tau_{n,k}(u))\big] \quad (1)$$

where the carrier frequency is ω_c (rad/s) with bandwidth B (Hz) and the variables (t, u) represent fast-time within a pulse and the SAR platform position respectively. The delay to the n^{th} channel is given by,

$$\tau_{n,k}(u) = \frac{1}{c}\left[R\left(x_k, y_k - u\right) + R\left(x_k, y_k - u - d_n\right)\right] \quad (2)$$

where $R(\cdot,\cdot)$ is the distance to the patch and the antenna offset $d_n = (n-1)\delta$ for antenna spacing δ with $n \in [-(N-1)/2, (N-1)/2]$ for N (odd) antenna elements. In the fast-time frequency domain $\omega \in [\omega_c - B\pi, \omega_c + B\pi]$, this expression becomes

$$s_{n,k}(\omega,u) = \sigma_k \exp\left[-j\omega\tau_{n,k}(u)\right]. \quad (3)$$

If the SAR is being jammed by an airborne platform, there will be two extra signal components required in the data model, the direct-path and the ground reflected path (hot-clutter). Consider the following geometry in Figure 1. The direct-path distance is given by $R_{d,0}$, the distance from the jammer platform to the k^{th} patch by $R_{j,k}$ and the k^{th} patch to the SAR platform by $R_{p,k}$. Unit vectors in each direction are indicated by $\hat{\mathbf{R}}_{d,0}$, $\hat{\mathbf{R}}_{j,k}$ and $\hat{\mathbf{R}}_{p,k}$.

The bistatic jammer model is adapted from [2] and assumes there are K hot-clutter patches within a given area. If an absolute time variable, $\tilde{t} = u/v_p + t$ is defined as the sum of slow-time and fast-time, then the output of the n^{th} receiver, $z_n(\cdot)$, is the superposition of the delayed reflectors for each patch,

$$z_n(t,u) = \sum_{k=0}^{K} b_k j(\tilde{t} - \tilde{\tau}_{n,k}(t,u)) \quad (4)$$

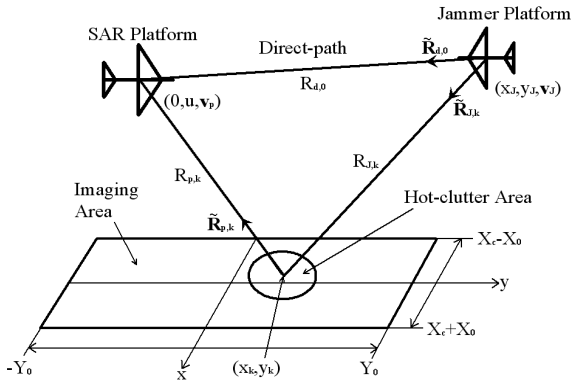

Figure 1: Jammer Geometry

where $j(\cdot)$ is the jamming signal, $\tilde{\tau}_{n,k}(\cdot)$ is the bistatic delay and b_k is the relative magnitude between the direct and reflected paths with the direct-path power set to unity ($b_0 \equiv 1$) and for $k > 0$,

$$b_k = \left(\frac{G_{r,k}}{G_{r,0}}\frac{\sigma_k A_k}{4\pi}\right)^{1/2} \frac{R_{d,0}}{R_{p,k}R_{j,k}}, \quad k > 0 \qquad (5)$$

where A_k is the effective area, σ_k the bistatic RCS, and $G_{r,0}$ and $G_{r,k}$ are the transmit and receive gains for each direction. Equation (4) can be simplified using the standard narrow-band assumption which implies that the jammer signal can be written as a separable function,

$$z_n(t,u) = \sum_{k=0}^{K} b_k j(\tilde{t}) \exp[-j\omega_c \tilde{\tau}_{n,k}(t,u)]. \qquad (6)$$

The hot-clutter distribution is modelled with a specular component at the center of the ground patch and $(K-1)$ diffuse components surrounding it. The RCS is modelled with a two-dimension gaussian distribution with independent x and y variables. For each pulse, the location of both platforms change and the hot-clutter patch varies position on the ground. This implies that each hot-clutter scatterer will have a different position for each pulse.

3 Effect of Hot-clutter on SAR

If these models are combined in a simple simulation, the effect of hot-clutter on a SAR image can be seen. The parameters chosen are summarised in Table 1 and a comparison between a synthetic SAR arrow image and the same image with hot-clutter added are shown in Figure 2. For azimuth focussing, a multichannel Spatial Matched Filter/Interpolation algorithm is used, [4].

The hot-clutter has severely degraded the SAR image in Figure 2. To quantify this, a number of image metrics are presented in section 6 and applied to the SAR images with varying hot-clutter power levels.

Table 1: Simulation Parameters

Parameters	**Value**
Carrier Frequency / Bandwidth	10 / 0.3 GHz
Number of Elements / Spacing	5 / $\frac{\lambda}{2}$ m
PRI / Platform Velocity	1 ms / 50 ms^{-1}
Range / Azimuth Resolution	1 / 0.2 m
Range Center / No. Fast-time Avgs	40 m / 5
No. Hot-clut. Scats.	100
SAR Imaging Area - Arrow	
Direct Path Power	75dB
Number of Pulses / Range Bins	136 / 134
SAR Imaging Area - Pt. Target	
Direct Path Power	20dB
Number of Pulses / Range Bins	128 / 106

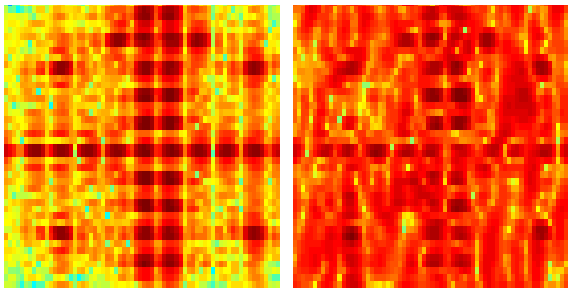

Figure 2: Image Comparison

4 Slow-time STAP for Stationary Jammer Suppression

The principle cause of non-stationarity is due to the relative motion between the two platforms and the changing super-position of the direct-path and terrain scattered components of the interference. The degree of non-stationarity will depend on the relative power between these components as well as the geometrical and physical features of the ground which varies in each pulse. If the relative power of the direct-path signal is much greater then the terrain scattered component, the total interference can be classed as 'approximately stationary' and less intensive filtering using slow-time STAP algorithms may be sufficient to remove the predominant interference.

To focus an image in azimuth, a slow-time steering vector is required to determine the response for each focussing position. This is typically done in the fast-time frequency domain (ω, u) using equation (3) with unity RCS,

$$s_n(\omega,u) = \exp\left[-j\omega\tau_n(u)\right] \qquad (7)$$

and the central range X_c chosen as a range reference,

$$\tau_n(u) = \frac{1}{c}\left[R\left(X_c,u\right) + R\left(X_c,u-d_n\right)\right]. \qquad (8)$$

To maintain the phase center at the center of the synthetic array, the SAR sample positions are referenced by $m \in [-(M-1)/2, (M-1)/2]$. Slow-time filtering is then accomplished by a convolution over all pulses. If

the slow-time steering vector and the data vector are first spatially stacked and then stacked over pulse delays,

$$\mathbf{s}(\omega, u-u_m) = [s_1(\omega, u-u_m), \ldots, s_N(\omega, u-u_m)]^T \in \mathcal{C}^{N\times 1},$$
$$\mathbf{S}(\omega, u) = [\mathbf{s}(\omega, u-u_1), \ldots, \mathbf{s}(\omega, u-u_M)]^T \in \mathcal{C}^{MN\times 1}$$

then the following equations can be written,

$$y(\omega, u) = \sum_{m=1}^{M} \mathbf{s}^H(\omega, u-u_m)\mathbf{x}(\omega, u_m) = \mathbf{S}^H(\omega, u)\mathbf{X}(\omega) \quad (9)$$

where $X(\omega)$ represents the stacked multichannel SAR data in the (ω, u) domain. Optimal slow-time STAP involves replacing the slow-time steering vector with the optimal weight for each frequency,

$$\tilde{y}(\omega, u) = \mathbf{W}^H(\omega, u)\mathbf{X}(\omega) \quad (10)$$

where

$$\mathbf{W}(\omega, u) = \hat{\mathbf{R}}_{\mathbf{I}}^{-1}\mathbf{S}(\omega, u) \in \mathcal{C}^{MN\times 1} \quad (11)$$

and the interference space-time covariance is determined by a Sample Matrix Inverse (SMI) estimated over L frequency bins with 0dB of additive noise ($\sigma_n^2 = 1$) to regularise the covariance estimate,

$$\hat{\mathbf{R}}_{\mathbf{I}} = \frac{1}{L}\sum_{l=1}^{L} \mathbf{Z}(\omega_l)\mathbf{Z}^H(\omega_l) + \sigma_n^2 I_{NM} \in \mathcal{C}^{MN\times MN} \quad (12)$$

It is assumed that techniques as described in [5] and [1], can be used to get a interference plus noise only estimate of the covariance matrix and hence $\mathbf{Z}(\cdot)$ is obtained from signal free data. The final step to form a SAR image is to perform range migration compensation by using Stolt interpolation as described in [4].

5 Fast-time STAP for Hot-clutter suppression in SAR

Filtering SAR data in fast-time is slightly different as it is not focussing in azimuth, but rather beamforming the spatial channels for each pulse. The form of the fast-time steering vector is therefore similar to equation (1) with unity RCS and a spatial delay only,

$$\bar{s}_n(t, u) = \exp\left[-j\omega_c \bar{\tau}_n(u)\right] \mathrm{sinc}\left[B\pi(t - \bar{\tau}_n(u))\right] \quad (13)$$

where

$$\bar{\tau}_n(u) = \frac{1}{c}\left[R\left(X_c, u + d_n - d_1\right) - R\left(X_c, u\right)\right]. \quad (14)$$

Note that the spatial delays are relative to the first antenna since the fast-time samples are not centered in phase as the slow-time samples were. Also, $\bar{\tau}_n(u)$ is practically independent of u and hence fast-time STAP is essentially forming a broadside beam at each pulse while nulling the interference.

Similarly to slow-time focussing, fast-time filtering is accomplished by a convolution over all range bins. If the fast-time steering vector and the data vector are first spatially stacked and then stacked over range bins,

$$\bar{\mathbf{s}}(t-t_l, u) = [\bar{s}_1(t-t_l, u), \ldots, \bar{s}_N(t-t_l, u)]^T \in \mathcal{C}^{N\times 1},$$
$$\bar{\mathbf{S}}(t, u) = [\bar{\mathbf{s}}(t-t_1, u), \ldots, \bar{\mathbf{s}}(t-t_L, u)]^T \in \mathcal{C}^{LN\times 1}$$

then the following equations can be written,

$$\bar{x}(t, u) = \sum_{l=1}^{L} \bar{\mathbf{s}}^H(t-t_l, u)\mathbf{x}(t_l, u) = \bar{\mathbf{S}}^H(t, u)\mathbf{X}(u). \quad (15)$$

Optimal fast-time STAP involves replacing the fast-time steering vector with the optimal weight for each pulse,

$$\tilde{x}(t, u) = \bar{\mathbf{W}}^H(t, u)\mathbf{X}(u) \quad (16)$$

where

$$\bar{\mathbf{W}}(t, u) = \hat{\mathbf{R}}_{\mathbf{I}}^{-1}\bar{\mathbf{S}}(t, u) \in \mathcal{C}^{LN\times 1} \quad (17)$$

and the interference covariance is now determined by running SMI average over the previous M' pulses. For example, on the m^{th} pulse, $\Omega_m \in [m - M' + 1 : m]$. The covariance is again whitened with 0dB of noise to avoid a non-singular inverse.

$$\hat{\mathbf{R}}_{\mathbf{I}} = \frac{1}{M'}\sum_{\Omega_m} \mathbf{Z}(u_m)\mathbf{Z}^H(u_m) + \sigma_n^2 I_{LN} \in \mathcal{C}^{LN\times LN} \quad (18)$$

Figure 3 represents an overview of fast-time STAP.

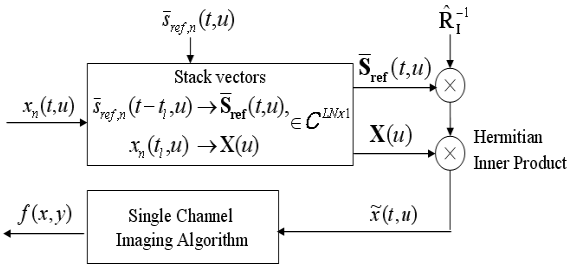

Figure 3: Fast-time STAP Block Diagram

6 Image Comparisons

To obtain a quantitative measure of image degradation, the Signal to Interference plus Noise Ratio (SINR) and Mean Square Error (MSE) can be calculated. Let $Y(x_p, y_q)$ denote either the conventional, slow-time STAP or fast-time STAP images described above in the presence of signal, jammer and noise for image pixels $p = 1 \ldots P, q = 1 \ldots Q$. Corresponding, $D(x_p, y_q)$ denotes the image in the presence of just the signal. The SINR is then defined as

$$SINR = \frac{\sum_{p,q} |D(x_p, y_q)|^2}{\sum_{p,q} |Y(x_p, y_q) - D(x_p, y_q)|^2} \quad (19)$$

and the MSE by,

$$MSE = \frac{1}{PQ}\sum_{p,q} |Y(x_p, y_q) - D(x_p, y_q)|^2. \quad (20)$$

To provide a greater degree of accuracy, each of these metrics will be averaged over five iterations. Figure 4 presents the averaged values of SINR and MSE when

the relative power of the hot-clutter interference is varied. For the fast-time STAP algorithm, the hot-clutter covariance is averaged over five pulses $(M' = 5)$. The three plots show how the arrow SAR image degrades and then how effective slow-time and fast-time STAP are at removing the interference.

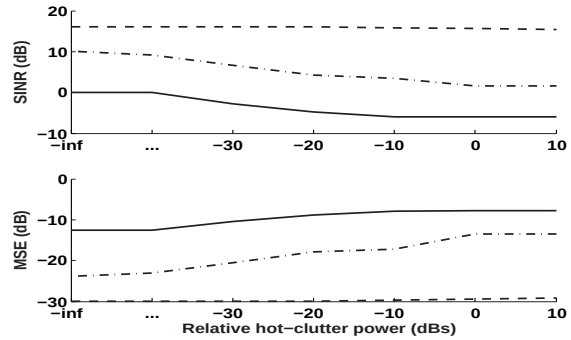

Figure 4: SINR and MSE Comparisons for Conventional Imaging (–), Slow-time STAP (-.-) and Fast-time STAP (- -)

As the relative hot-clutter power level is increased for the three cases, the SINR decreases and the MSE increases accordingly. While the slow-time STAP offers an improvement, the best suppression is achieved by fast-time STAP which maintains good performance independent of the strength of the hot-clutter.

To further quantify the effect of the interference, the Point Spread Function (PSF) of a single scatterer can be analysed. The Peak Sidelobe Ratio (PSR) and the Integrated Sidelobe Ratio (ISLR) can be used to determine the difference between the main-lobe and greatest sidelobe and the ratio of all energy in the sidelobes to the energy in the mainlobe. Figure 5 shows a comparison of the ISLR and PSR for a single point scatterer as the relative hot-clutter power is varied. The damaged image is again compared to the recovered image using slow-time and fast-time STAP. As the range PSR and ISLR remain almost constant for each of the three cases, only the azimuth ratio's were analysed.

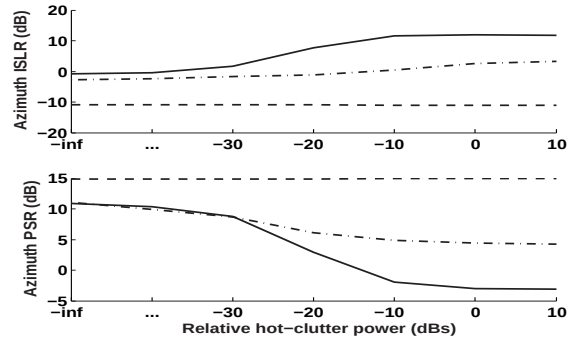

Figure 5: ISLR and PSR Comparisons for Conventional Imaging (–), Slow-time STAP (-.-) and Fast-time STAP (- -)

As expected when the interference level increases, the ISLR increases while the PSR decreases. Slow-time STAP offers some improvement, though is outperformed by fast-time STAP.

7 The Effect of Fast-time STAP

The use of fast-time STAP results in two unwanted modulations, training and coherency [3] as described in the introduction. Training modulation was investigated using only the direct-path signal as it represents a spatially stationary environment. To view the training modulation, Figure 6 shows the PSF of with only the direct-path was run with no averaging $(M' = 1)$ and with significantly more averaging $(M' = 32)$.

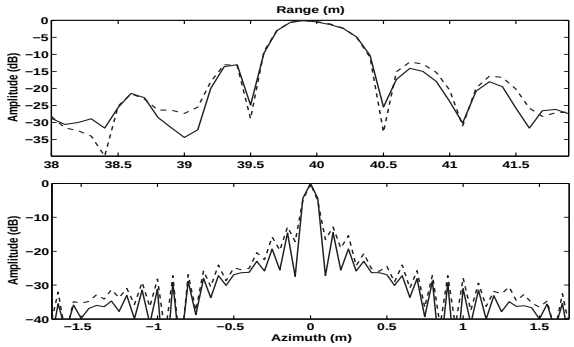

Figure 6: PSF for $M' = 1$ (–) and $M' = 32$ (- -)

Averaging over a greater number of pulses has the effect of raising the sidelobes of the PSF and skewing the range slice to the left. Though the effect is noticeable, the corruption is only small, indicating that the training modulation adds only a minor distortion to the SAR image.

8 Conclusion

This paper has demonstrated how hot-clutter can degrade a SAR image and that while slow-time STAP can recover the image, fast-time STAP is far more effective. Finally, to reduce distortion in the recovered image, the choice of training data is important for fast-time STAP as it effects the amount of training modulations.

9 Literature

[1] J. Ender. Anti-jamming adaptive filtering for SAR imaging. In *DGON IRS'98*, 1998.

[2] R. L. Fante and J. A. Torres. Cancellation of diffuse jammer multipath by an airborne adaptive radar. *IEEE Transactions on Aerospace and Electronic Systems*, v31, no. 2, 1995.

[3] D. Rabideau. Clutter and jammer multipath cancellation in airborne adaptive radar. *IEEE Proceedings on Aerospace and Electronic Systems*, v36, no. 2, April 2000.

[4] L. Rosenberg and D. Gray. Multichannel SAR Imaging using Wavefront Reconstruction. In *International Radar Symposium Proceedings*, 2004.

[5] J. Ward. Space-Time Adaptive Processing for airborne radar. Technical report 1015, Lincoln Labs. MIT, 1994.